Journal of Energy Storage 72 (2023) 108610

Contents lists available at ScienceDirect

Journal of Energy Storage

journal homepage: www.elsevier.com/locate/est

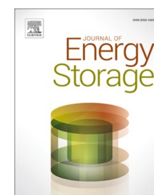

Research papers

A hybrid thermal management system combining liquid cooling and phase change material for downhole electronics

Jiale Peng, Chao Deng, Fulong Wei, Siqi Ding, Run Hu, Xiaobing Luo *

School of Energy and Power Engineering, Huazhong University of Science and Technology, Wuhan, China

ARTICLE INFO

Keywords:
Numerical simulation
Liquid cooling
Phase change material
Hybrid thermal management
Downhole electronics
Workable time

ABSTRACT

The electronics inside the logging tools are prone to failure due to the extreme thermal environments. In this study, a hybrid thermal management system using liquid cooling and phase change material (PCM) for downhole electronics is proposed to extend the workable time. In this system, a spiral pipe and a S-shaped pipe are respectively arranged inside the PCM and the cold plates to strengthen the heat exchange. To investigate the performance of this system, the transient flow and heat transfer simulation are implemented using finite element method. The accuracy is validated by comparing with the reported experimental results, showing an error of less than 6.7 %. The results show that the hybrid thermal management system increases the operating time of the electronics from 230 min to 450 min, which is attributed to the introduction of liquid cooling. The maximum temperature difference between the electronics and PCM reduces from 30 °C to 2 °C. Moreover, the effect of flow rate, spiral pipe spacing, heating power and ambient temperature on the temperature control performance are explored. This work provides a guidance for the design and optimization of logging tools, which is significative to shorten their research and development cycle.

1. Introduction

Logging tools are used to detect the distribution of petroleum resources underground in extreme thermal environments [1–3]. The ambient temperature might exceed 200 °C when the logging tool operates in a well with a depth of more than 5 km [4,5]. For specific instruments, the temperature of the downhole electronics inside the logging tool needs to be limited below 100 °C during working time [6]. Without thermal protection, the temperature of the electronics would quickly exceed the temperature limit due to the dual influence of high temperature environment and self-generated heat [7–9]. Hence, it becomes important to implement effective thermal management for the normal electronics to ensure their safe and stable operation.

The existing thermal management measures can be mainly divided into active thermal management techniques (ATMT) and passive thermal management techniques (PTMT). The active thermal management techniques include vapor compression refrigeration [10–12], split-Stirling refrigerator [13,14], and thermoelectric refrigeration [15–17], which transport the heat generated by the electronics to the high temperature environment through external input energy. The ATMT shows the advantages of long temperature control time and adjustable cooling power. However, limited by the reliability, these ATMT systems are difficult to be applied in the actual operation of logging tools. Passive thermal management techniques mainly include thermal insulation, heat storage, and enhanced heat exchange [18–20]. First, high vacuum insulation and porous materials are used to reduce the heat intrusion from high-temperature environment to the internal electronics [21–23]. Second, phase change material (PCM) with high thermal conductivity and heat storage capacity are utilized to store the self-generated heat of electronics and the leaked heat from the external high-temperature environment [24–27]. Third, the electronics and PCM are connected by the thermal channels, which are composed of metals with high thermal conductivity, such as cooper and aluminum [20,28]. Benefitted from no additional energy input and no moving parts, passive thermal management systems show the highest reliability. However, the temperature difference between the electronics and PCM in passive thermal management systems remains large due to the limited heat transfer of the thermal channels, which limits the heat transfer and storage of PCM. Therefore, for passive thermal management systems, the PCM may be underutilized when the internal electronics reach their temperature limit, resulting in short working time.

In contrast, combining active and passive thermal management techniques can make full of the advantages of both to extend the

* Corresponding author.
E-mail address: luoxb@hust.edu.cn (X. Luo).

https://doi.org/10.1016/j.est.2023.108610
Received 14 April 2023; Received in revised form 14 July 2023; Accepted 2 August 2023
Available online 8 August 2023
2352-152X/© 2023 Elsevier Ltd. All rights reserved.

Nomenclature

ρ	density
c	specific heat capacity
λ	thermal conductivity
T	temperature
t	time
u	velocity of working liquid
P	pressure of working liquid
q	power per unit volume
μ	dynamic viscosity of working liquid
Re	Reynolds number
d	pipe diameter
L_m	latent heat of PCM
c_{eff}	equivalent heat capacity of PCM
θ	volume fraction of liquid PCM
V	volume
h_L	average convective heat transfer coefficient
r_h	radius of the wellbore wall
r_t	radius of the logging tool
L	length of the logging tool
a	thermal diffusion coefficient
φ	Reynold stress

Subscripts

s	solid materials
l	working liquid
in	inlet
out	outlet
PCM-s	solid PCM
PCM-l	liquid PCM
onset	start of phase change
end	end of phase change

operating time of electronics. Currently, liquid cooling technology has been relatively mature, and widely used in various fields due to the advantages of long-distance heat transfer and strong heat dissipation capacity [29–32]. In the few studies, the thermal channels have been replaced by liquid cooling for thermal management of downhole electronics, and good temperature control performance has been achieved. For example, Jakaboski [33] proposed an innovative thermal management of electronics used in oil well logging. At an ambient temperature of 205 °C, the system can maintain the temperature of electronics under 100 °C for approximately 28 h by liquid cooling. Ma et al. [34] proposed a thermal protection with insulation material and liquid cooling for using in deep downhole environments, which can extend the downhole electronics' operating time to 5 h. The above studies have provided qualified resolution for the thermal management under specific circumstances. However, on the one hand, the heat transfer between the electronics and PCM in the above study can be further enhanced by rational designs. And the selection of the PCM does not consider the actual initial ambient temperature, which may lead to underutilization of the latent heat of PCM. Due to the subcooling degree of the PCM, once the ambient temperature is higher than the solidification temperature of the PCM, the latent heat of the PCM cannot be recycled, resulting in safety issue [35]. On the other hand, the above thermal management systems for downhole electronics are designed empirically since no suitable numerical model has been available for numerical simulation due to complex heat transfer of the whole system. Once the experimental results do not meet the requirements, the system needs to be redesigned, and the prototype needs to be refabricated and retested, which greatly increase the research and development (R&D) cycle and cost. Therefore, first, it is urgent to propose a hybrid thermal management system, which both enhances heat transfer and takes into account the effect of the actual initial ambient temperature on the utilization of the PCM. Second, it is necessary to propose a numerical method to simulate the complex processes of the hybrid thermal management system for guiding the system design and cutting down the R&D cycle and cost.

In this study, a hybrid thermal management system (HTMS) for downhole electronics is proposed to prolong the workable time. This

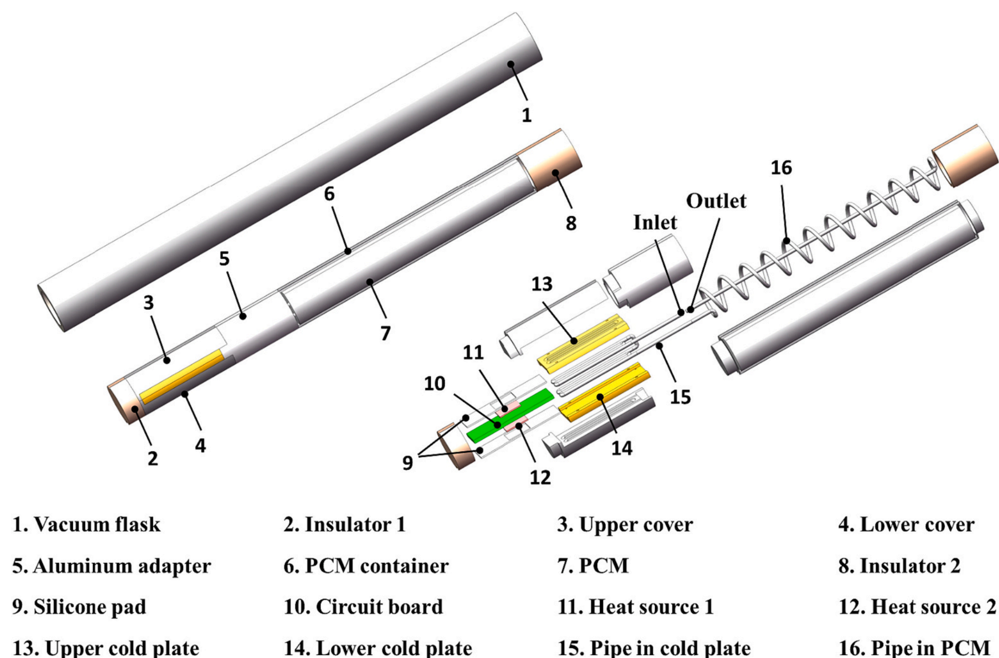

Fig. 1. The physical model of the HTMS for downhole electronics.

Table 1
Materials and thermal properties of the logging tool [41].

Name	Material	Thermal conductivity (W·m^{-1}·K^{-1})	Density (kg·m^{-3})	Heat capacity (J·kg^{-1}·K^{-1})
Vacuum bottle	Inconel 718	14.7	8240	436
Vacuum layer	Composite	0.0002	100	1200
Adapter and cover	Aluminum alloy 6061	167	2710	896
Cold plate	Copper	400	8700	385
Heat sources	Ceramic	30	3960	850
Heat-conductive silicone pads	Silica gel	1	1810	923
PCM	LMPA	18.79	9580	146(s)184(l)
PCM container and pipe	304	16.3	7930	500
Insulator shell	PEEK	0.25	2200	1000
Insulator core	Aluminum silicate wool	0.035	400	794.2
Working fluid	Deionized water	0.6	998	4128

system adopts liquid cooling and low melting point alloys (LMPA) for temperature control. Suitable LMPA is selected according to actual temperature requirements. A spiral pipe and a S-shaped pipe are respectively arranged inside the phase change material and the cold plate to strengthen heat exchange. To guide the system design of HTMS, first, the 3D model of the whole hybrid thermal management system is designed. Subsequently, a numerical heat transfer model of the whole system is constructed based on some reasonable simplification. Then, the numerical model is validated by reported experimental studies. The temperature control effect of the proposed system is compared with a conventional thermal management system using thermal channels for heat conduction. Finally, some factors affecting the performance of the proposed system are carefully studied.

2. Methods

2.1. System composition

Fig. 1 shows the physical model of the HTMS for downhole electronics combining liquid cooling and PCM under extreme thermal environment. The HTMS is composed of vacuum flask, insulator 1, upper cover, lower cover, aluminum adapter, PCM container, PCM, insulator 2, silicone pad, circuit board, electronics (regarded as heat source 1 and heat source 2), upper cold plate, lower cold plate and pipe and coolant. The vacuum flask is utilized to isolate circumferential heat transfer from high-temperature environment. The outer and inner diameters are 90 mm and 73 mm, respectively, with the length of 810 mm. The vacuum flask has a vacuum layer (3 mm) between the inner and outer diameter. Insulator 1 and insulator 2 are located at the open end and closed end for reducing axial heat transfer from high-temperature environment, respectively, with the length of 84 mm and the diameters of 72 mm.

The electronics are installed on the circuit board. The gaps among the circuit board and cold plates are filled with heat-conductive silicone pads. There are S-shaped flow channels between cold plates and cover plates for pipe arrangement to strengthen the heat exchange between the cold plates and pipe. The pipe containing coolant inside the PCM is spirally arranged for enhancing the heat transfer between the liquid and the PCM. The heat generated by the electronics can be quickly transferred to the cold plate through the heat-conductive silicone pads. Subsequently, the self-generated heat is stored in the PCM through liquid cooling. Aluminum adapter is used to connect the cover to the PCM container. Space is reserved inside the aluminum adapter for a pump and a fluid compensator, which are connected to the inlet and outlet, respectively. The outer and inner of pipe are 6 mm and 5 mm, respectively. The working fluid inside the pipe is deionized water, which can work stably below 100 °C. The ceramic heat plates are used to simulate heat sources with thermal conductivity of 30 W/(m·K), density of 3960 kg/m^3 and specific heat capacity of 850 J/(kg·K), respectively. The heat-conductive silicone pads are composed of silica gel with the thermal conductivity of 1 W/(m·K), density of 1810 kg/m^3 and specific heat capacity of 923 J/(kg·K), respectively. The detailed parameters of the other structures are shown in Table 1.

2.2. Numerical heat transfer model

In this section, the proposed thermal management system is simulated by finite element method. The heat transfer processes of the whole system include convection heat exchange between the slurry and the vacuum flask, multiple heat transfer mode in the vacuum layer, solid heat conduction, natural convection heat exchange, thermal radiation inside the vacuum flask, forced convection heat exchange through the coolant, phase change heat storage, etc. To simulate these heat transfer processes quickly and accurately, the following assumptions are made:

(1) The vacuum layer is equivalent to a solid layer with low thermal conductivity [36].
(2) Contact thermal resistance is ignored in the heat transfer process [20].
(3) The change of physical properties of materials with temperature is ignored [21].
(4) The electronics are regard as uniform heat sources.
(5) Natural convection and thermal radiation inside the vacuum flask are ignored [37].
(6) Coolant is considered as laminar and incompressible fluid.

After simplification, the heat transfer processes are divided into four parts: solid heat transfer, forced convection heat transfer through liquid cooling, phase change heat storage process, and convection heat transfer from the high-temperature mud to the vacuum flask.

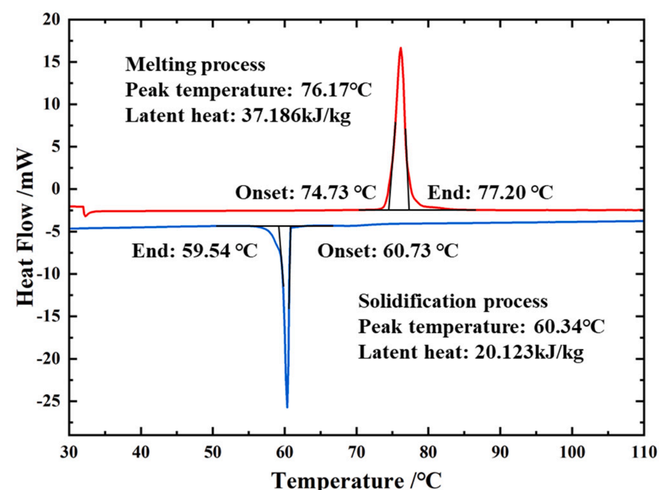

Fig. 2. The DSC test curve of selected LMPA.

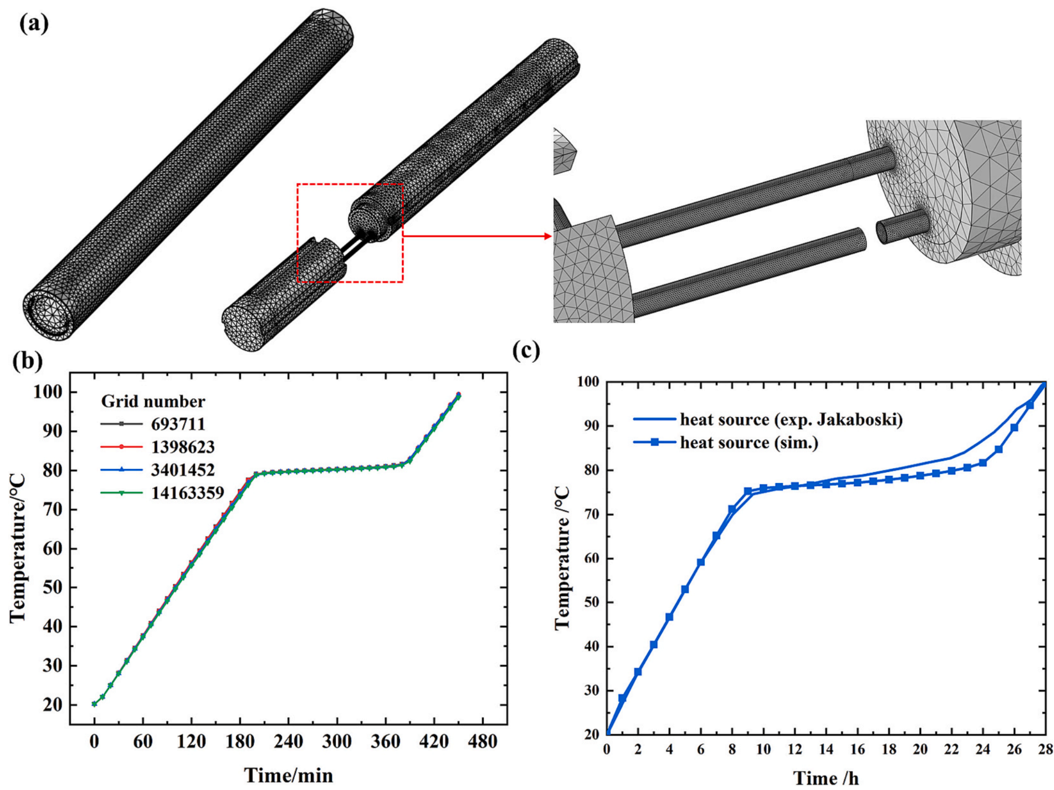

Fig. 3. Grid-independent validation and numerical method validation. (a) grid division diagram; (b) the temperature-rising curves for different grid numbers; (c) the heat source temperature curves versus time.

The solid heat transfer process can be expressed as [38]:

$$\rho_s c_s \frac{\partial T}{\partial t} = \nabla \cdot (\lambda_s \nabla T) + q \tag{1}$$

For the forced convection heat transfer through liquid cooling, the continuity equation can be expressed as [39]:

$$\frac{\partial \rho_l}{\partial t} + \nabla \cdot (\rho_l \boldsymbol{u}) = 0 \tag{2}$$

The conservation of momentum equation can be expressed as:

$$\rho_l \frac{\partial \boldsymbol{u}}{\partial t} + \rho_l (\boldsymbol{u} \cdot \nabla) \boldsymbol{u} = -\nabla P + \mu \nabla^2 \boldsymbol{u} - \varphi \tag{3}$$

To simulate the liquid cooling cycle accurately and quickly, the pump and liquid compensator are equivalent to the inlet and outlet of the cycle, respectively. The inlet is the velocity boundary condition generated by the pump, and the outlet is the pressure boundary condition of the fluid flowing back to the liquid compensator. To ensure temperature continuity, the temperature of the liquid inlet and outlet are kept the same at every moment, which can be expressed as:

$$T_{in} = T_{out} \tag{6}$$

For the phase change heat storage process, it is calculated by the equivalent heat capacity method [40], which can be expressed as:

$$c_{eff} = \begin{cases} c_{PCM-s} & (T < T_{\text{onset}}) \\ \frac{1}{\rho}\left[(1-\theta)\cdot\rho_{PCM-s}\cdot c_{PCM-s} + \theta\cdot\rho_{PCM-l}\cdot c_{PCM-l}\right] + \frac{L_{\text{m}}}{T_{end} - T_{onset}} & (T_{onset} \le T \le T_{end}) \\ c_{PCM-l} & (T_{end} < T) \end{cases} \tag{7}$$

The conservation of energy equation for the heat transfer process can be expressed as:

$$\rho_l c_l \frac{\partial T_l}{\partial t} + \nabla \cdot (\rho_l c_l \boldsymbol{u} T_l) = \nabla \cdot (\lambda_l \nabla T_l) \tag{4}$$

The flow form is determined by the Reynolds number, which is expressed as:

$$Re = \frac{\rho_l u d}{\mu} \tag{5}$$

where, θ is a function of temperature. It can be expressed as:

$$\theta = \begin{cases} 0 & (T < T_{onset}) \\ \frac{V_{PCM-l}}{V_{PCM-l} + V_{PCM-s}} & (T_{\text{onset}} \le T \le T_{end}) \\ 1 & (T_{end} < T) \end{cases} \tag{8}$$

The equivalent density can be expressed as:

$$\rho_{PCM} = (1-\theta)\cdot\rho_{PCM-s} + \theta\cdot\rho_{PCM-l} \tag{9}$$

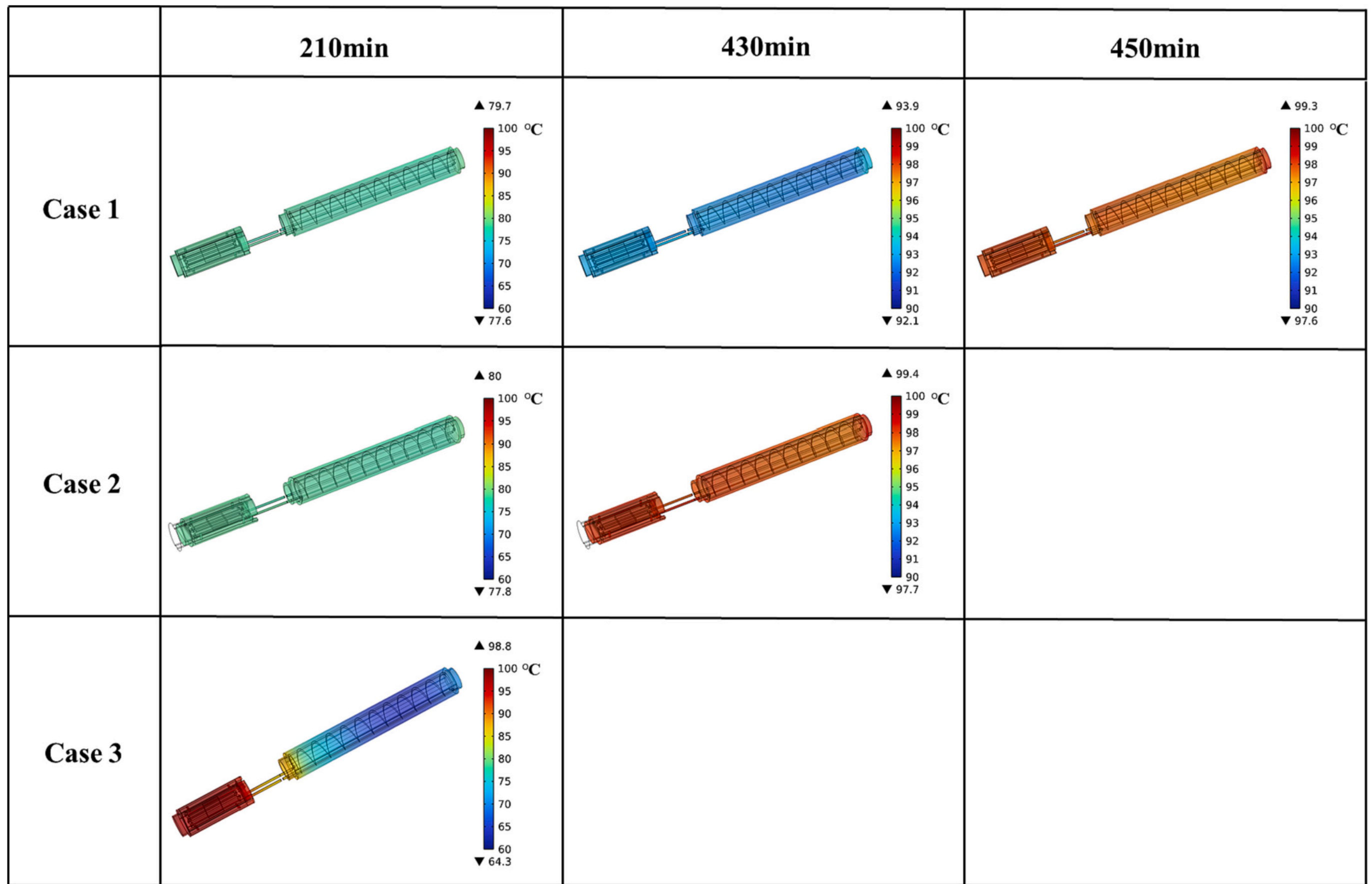

Fig. 4. The temperature distribution of different heat transfer modes at different moment.

The equivalent thermal conductivity can be expressed as:

$$\lambda_{PCM} = (1-\theta)\cdot\lambda_{PCM-s} + \theta\cdot\lambda_{PCM-l} \tag{10}$$

For the convection heat transfer from the high-temperature mud to the vacuum flask, the average convective heat exchange coefficient can be expressed as [37]:

$$h_L = \frac{1}{L}\int_0^L h(x) = \frac{3\lambda_{\text{mud}}}{4}\left[\frac{U}{45(r_h - r_t)^2 aL}\right]^{\frac{1}{3}}\left[(11r_h - 5r_t)^{\frac{1}{3}} + \left(\frac{29r_h - 5r_t}{16}\right)^{\frac{1}{3}}\right] \tag{11}$$

2.3. Selection of PCM

PCM, usually referred to solid-liquid PCM, plays a key role in heat storage in the logging tool. The phase transition heat storage accounts for a large proportion of total heat storage. Therefore, the melting temperature should be as low as possible to make full use of the phase transition heat storage. Meanwhile, since the logging platforms are located all over the world, the temperature on the platforms may reach 50 °C. The PCM needs to maintain at solid state at this temperature to ensure the safety of the next logging. PCM usually has a certain degree of supercooling, which results that temperature interval of the solidification process doesn't coincide with the melting process interval. Hence, the solidification temperature of PCM should exceed the ambient temperature. Hence, it is necessary to select PCM with high heat storage capacity and high thermal conductivity. LMPA is a suitable PCM for thermal management of downhole electronics due to its high thermal conductivity and considerable latent heat. Fig. 2 shows the DSC test curves of the selected LMPA. The melting interval and solidifying interval of the LMPA are 74.73 °C–77.20 °C and 59.54 °C–60.73 °C, respectively. In addition, the latent heat of melting process can reach 37.186 kJ/kg, with the thermal conductivity of 18.79 W/(m·K).

2.4. Simulation setup and model validation

The software COMSOL was used to simulate the heat transfer process of this system. The control equations were first imported into the CFD solver, and then the 3D model was introduced into the solver to generate the mesh. The meshes of the pipe and fluid domain were partially encrypted, as shown in Fig. 3(a). Subsequently, the materials and the thermal properties of each component were defined according to Table 1. The viscosity of coolant was set to 0.001003 Pa·s. Several boundary conditions were set as follows. First, the downhole high temperature environment was set to convective heat exchange conditions. Second, the liquid cooling cycle inlet and outlet were set as velocity boundary condition and pressure boundary condition, respectively. Third, the outlet and inlet temperature were kept the same to ensure temperature continuity. Finally, the simulations were calculated for a certain time with the heat source temperature not exceeding 100 °C, and a time step of 10 min. In addition, several factors affecting the performance of the proposed system were carefully studied. Transient flow and heat transfer of the proposed system were simulated simultaneously.

To obtain the accurate calculations, grid-independence verification was performed. Fig. 3(b) shows the temperature-rising curves for different grid numbers. Considering the computational accuracy and time, grid number of 1,398,623 was selected for the subsequent simulations. Meanwhile, to verify the accuracy of the numerical method, a numerical model of the reported experimental study [33] was established whose simulated results were compared with the experiment. Fig. 3(c) shows the heat source temperature curves versus time. The

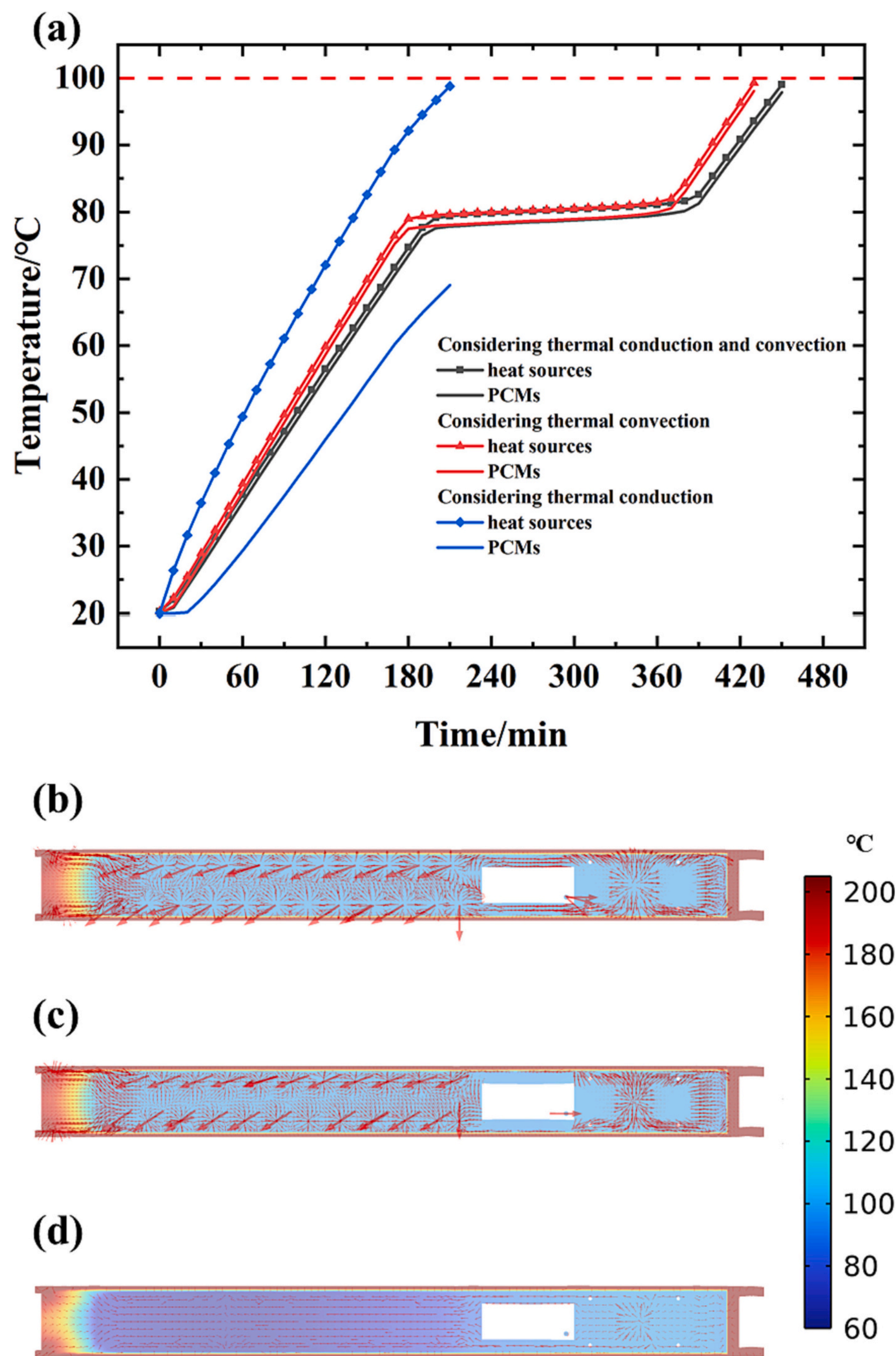

Fig. 5. The temperature curves and heat flow distribution. (a) the temperature curves of electronics for different heat transfer modes versus time; The heat flow distribution for different heat transfer modes, (b) case 1, (c) case 2, and (d) case 3. (For interpretation of the references to colour in this figure, the reader is referred to the web version of this article.)

maximum error between numerical results and reported experiment did not exceed 5 °C, and the maximum percentage deviation was less than 6.7 %, which validated the high accuracy of the numerical simulation method.

3. Results and discussion

3.1. Comparison with conventional heat transfer

Heat conduction through thermal channels is the conventional heat transfer mode between electronics and PCM. Fig. 4 shows the temperature distribution for different heat transfer modes at different moment. The heat transfer modes from electronics to PCM in case 1 include forced convective heat transfer through pipe and heat conduction through aluminum adapter. Case 2 and case 3 consider forced convective heat transfer through the pipes and heat conduction through the aluminum adapter, respectively. The inlet flow rate in liquid cooling system is 0.5 m/s. The spiral pipe spacing inside the PCM is 40 mm. The heating power is 30 W, and the ambient temperature is 205 °C. The temperature distribution in case 1 and case 2 are more uniform than that in case 3. In

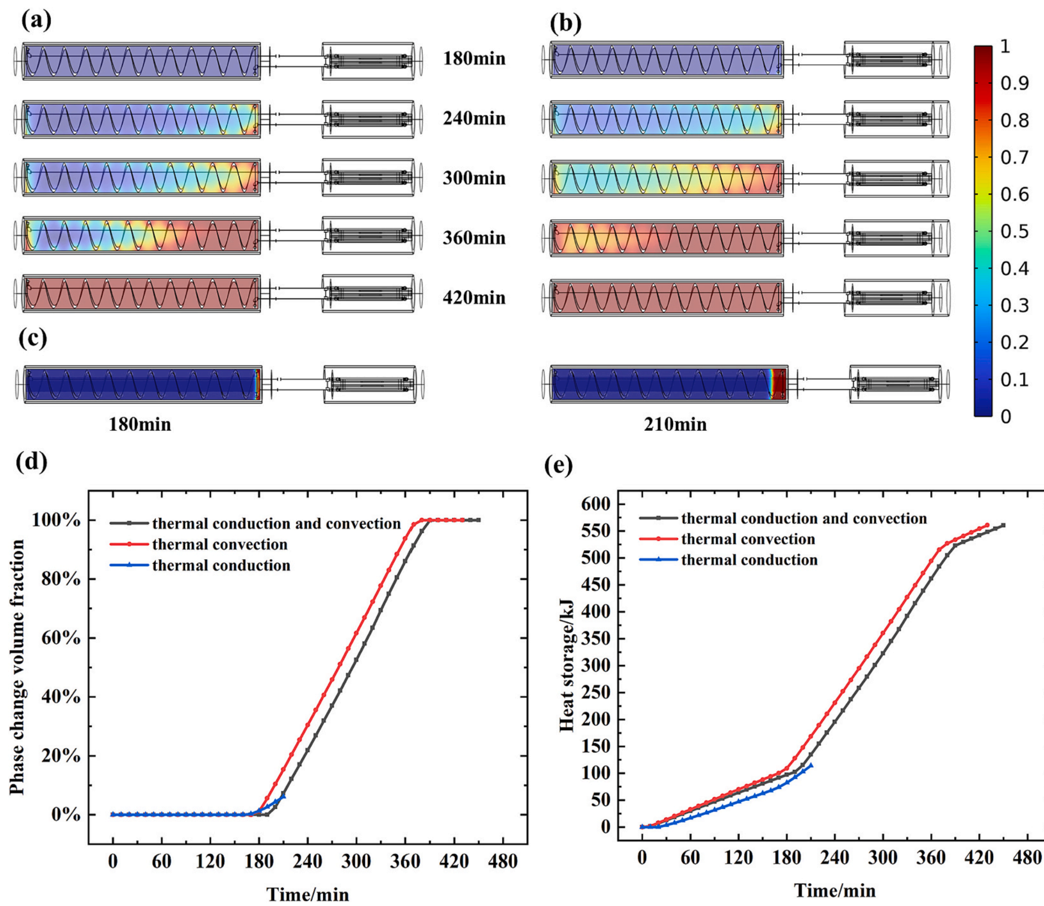

Fig. 6. The phase change and heat storage. The phase change with time for PCM of (a) case 1, (b) case 2 and (c) case 3; (d) the phase change volume fraction with time for different transfer modes; (e) the heat storage of PCM for different transfer modes.

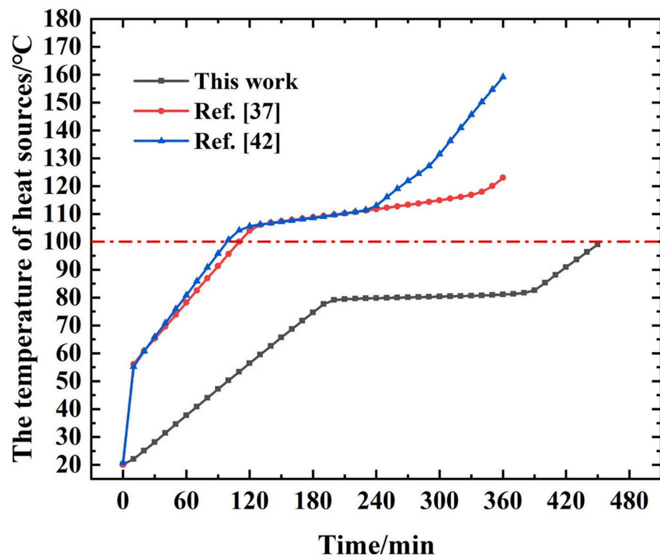

Fig. 7. The comparison with previous researches.

case 1, case 2 and case 3, the maximum temperature of the heat sources reaches the temperature limit at 210 min, 430 min and 450 min, respectively.

Fig. 5(a) shows the temperature curves for different heat transfer modes. When considering only the heat transfer through the aluminum adapter, the maximum temperature difference between the heat sources and PCMs reaches 30 °C. When the heat transfer through the pipes is considered, this temperature difference is reduced to within 2 °C, and the temperature curve possesses a clear constant temperature stage. In addition, when only the heat transfer through the pipes is regarded, the maximum temperature difference between the heat sources and PCMs is also within 2 °C, but the phase change interval is significantly advanced. Fig. 5(b)–(d) show the heat flow distribution for different heat transfer modes, where the colours indicate the temperature and the red arrows indicate the direction and size of the heat flow. Fig. 6(b)–(d) represent the heat transfer paths of case 1, case 2 and case 3, respectively. As shown in Fig. 6(b), most of the heat from the heat sources is dissipated to the cold plates, and then transferred to the PCM for storage through pipes and adapter, respectively. Compared to case 2 and case 3, the increased heat transfer pathways explain the longer workable time considering both heat conduction and heat convection. It can be derived from the size of the arrows that the heat flow through the pipe is much larger than that through the adapter. The thermal convection of the pipe dominates the entire heat dissipation process of the heat sources. Therefore, the temperature difference between the heat sources and PCM in case 1 and case 2 is almost the same.

Fig. 6(a)–(c) show the phase change with time for PCM of case 1, case 2 and case 3, respectively. 0 and 1 indicate the solid PCM and the liquid PCM, respectively. 0–1 indicate the solid-liquid mixing area of PCM, which reflects the phase change interface. In case 1 and case 2, the phase change of PCM starts from the nearby of the pipe and gradually spreads around. All the PCM eventually completes the phase change, when the heat source approaches the temperature limit. However, in case 3, the PCM begins the phase transition from the edge to the middle. Most of the PCM has not yet undergone phase change when the temperature of heat

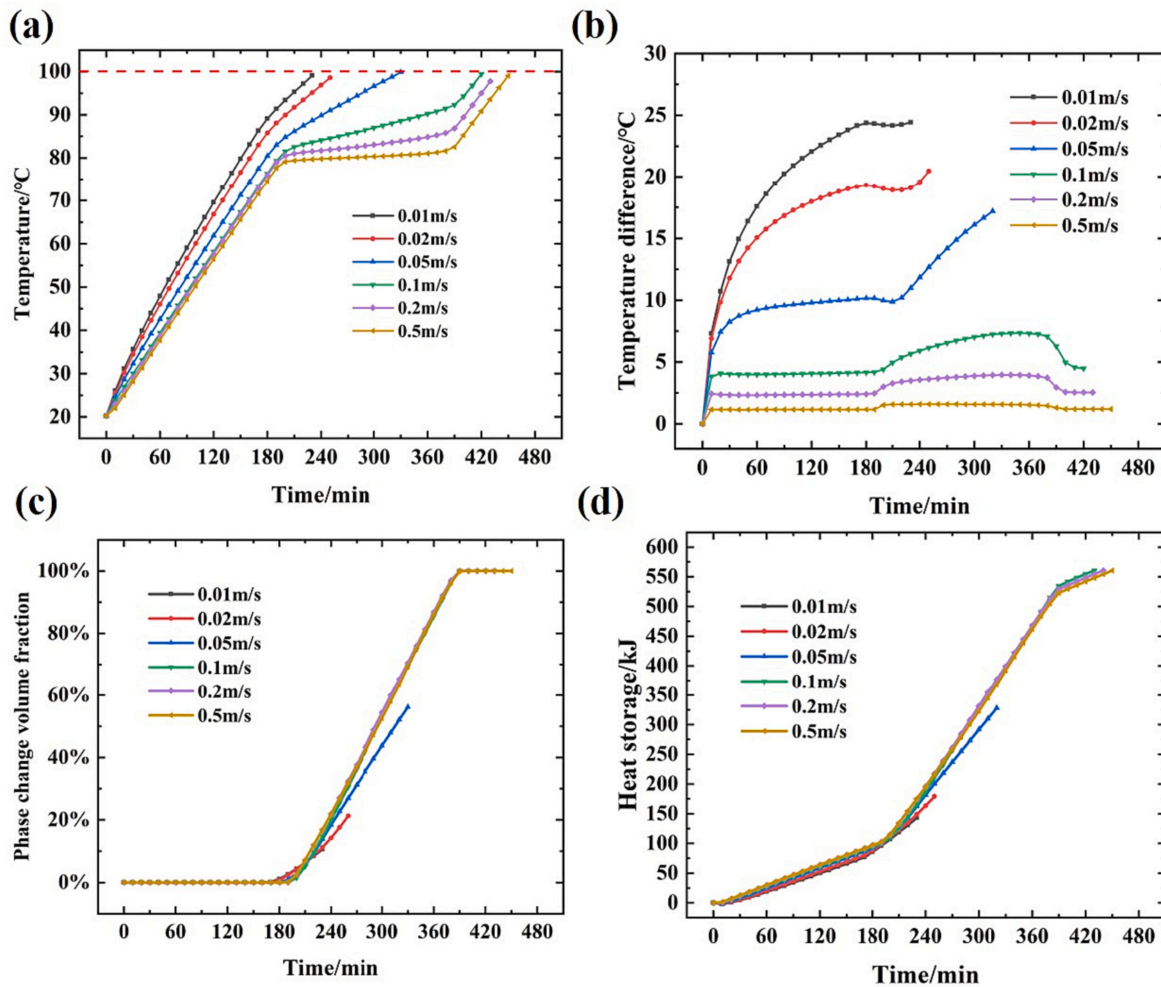

Fig. 8. (a) The temperature-rising of the electronics with time for different flow rate; (b) the temperature difference between the electronics and PCM with time for different flow rate; (c) the phase change volume fraction with time for different flow rate; (d) the heat storage of PCM with time for different flow rate.

sources approaches 100 °C. Fig. 6(d) shows the phase change volume fraction with time for different heat transfer modes. The inflections represent the beginning and completion of the phase transition, respectively. The phase transition intervals for case 1 and case 2 are 190–400 min and 180–380 min, respectively. Since the heat from the heat source is partially absorbed by the adapter, the phase transition in case 1 is delayed, resulting in relatively less heat absorption by the PCM. In case 3, the phase transition starts from 170 min, but the final phase change volume fraction is only 6.1 %. The heat transfer thermal resistance through the heat conduction of the adapter is too large, and the heat from heat sources is difficult to be absorbed quickly by the PCM. Fig. 6(e) shows the heat storage of PCM for different heat transfer modes. The heat storage rate is significantly increased in the phase change interval. The final PCM heat storage in case 1 reaches 560.35 kJ.

Fig. 7 shows the comparison of previous researches with this work. It is worth noting that in previous researches, the vacuum flask and the internal space, the heating power and ambient temperature are the same as in this work [37,42]. And passive thermal management combined with PCM was used in previous researches. In previous researches, the temperature of the heat sources rapidly exceeds 100 °C within 120 min, and then the temperature is maintained at about 110 °C due to the phase change of PCM. The temperature difference between the heat sources and PCM is more than 30 °C. In this work, the temperature of the heat sources is maintained below 100 °C for a long time, and the temperature difference between the heat source and the PCM does not exceed 2 °C.

Overall, the liquid cooling cycle can significantly reduce the heat transfer thermal resistance from the heat source to the PCM, and extend the electronics' workable time. The subsequent studies are carried out based on case 1.

3.2. *Effect of flow rate*

The effect of the flow rate on the proposed system can be analysed by changing the inlet flow rate of the coolant. Fig. 8(a) shows the temperature-rising of the electronics with time for different flow rate. The temperature-rising curve goes through two stages or three stages. As the flow rate increases from 0.01 m/s to 0.5 m/s, the temperature-rising rate of electronics in the first stage decreases from 23.33 °C/h to 19.21 °C/h, and in the second stage it decreases from 12.73 °C/h to 2.90 °C/h. The third stage occurs only with the flow rate not less than 0.1 m/s. In the third stage, the temperature-rising rate of the electronics increases to 16.46 °C/h at a flow rate of 0.5 m/s. When the flow rates are 0.01 m/s, 0.02 m/s, 0.05 m/s, 0.1 m/s, 0.2 m/s, 0.5 m/s, the workable time of the electronics are 230 min, 250 min, 320 min, 420 min, 430 min, 450 min, respectively. Fig. 8(b) shows the temperature difference between the electronics and PCM with time for different flow rate. The flow rate increases from 0.01 m/s to 0.1 m/s, and the maximum temperature difference between the electronics and the PCM is drastically reduced from 24.43 °C to 7.3 °C. When the flow rate increases further, the temperature difference decreases slowly. The maximum temperature

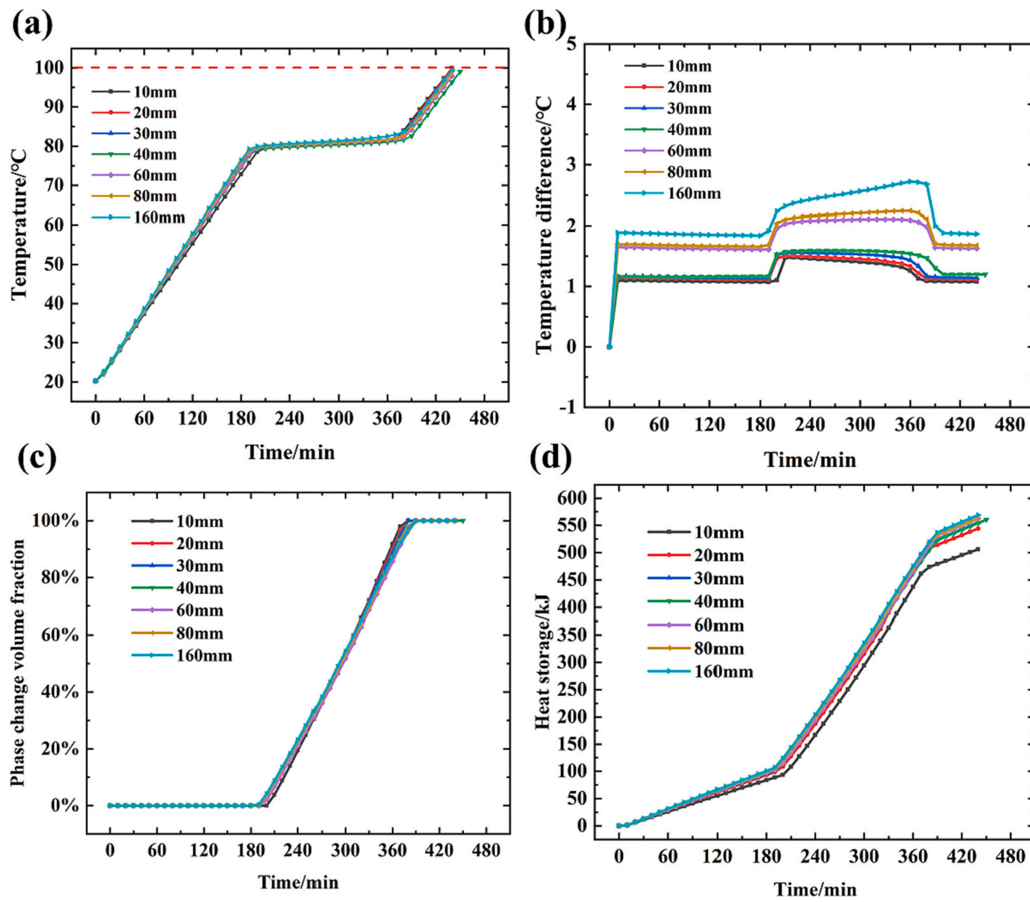

Fig. 9. (a) The temperature-rising of the electronics with time for different spiral pipe spacing; (b) the temperature difference between the electronics and PCM with time for different spiral pipe spacing; (c) the phase change volume fraction with time for different spiral pipe spacing; (d) the heat storage of PCM with time for different spiral pipe spacing.

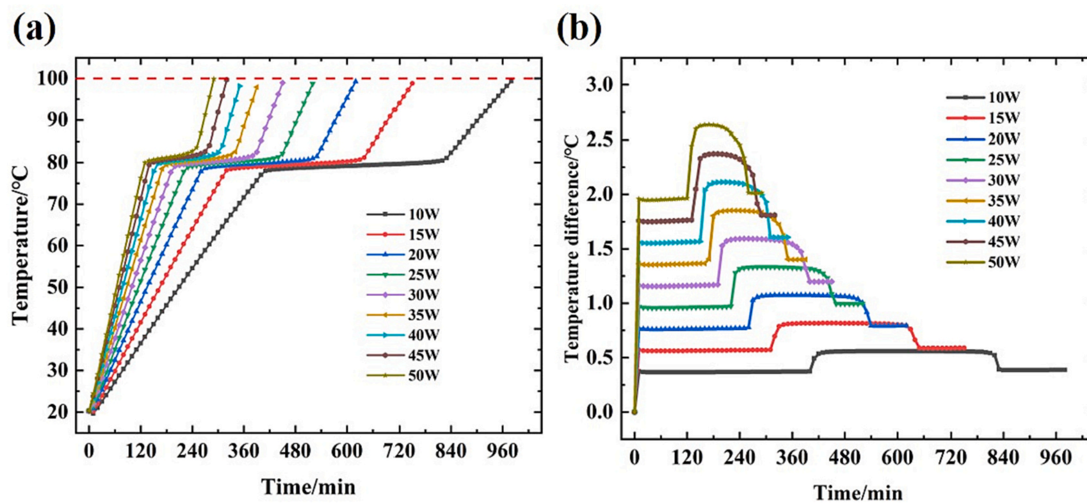

Fig. 10. (a) The temperature-rising of the electronics with time for different heating power; (b) the temperature difference between the electronics and PCM with time for different heating power.

difference is only 1.59 °C with the flow rate of 0.5 m/s. The temperature difference between the electronics and PCM increases abruptly around 200 min due to the occurrence of phase change.

Fig. 8(c) displays the phase change volume fraction with time for different flow rate. The slope represents the speed of the phase transition of PCM. The phase change rate gradually becomes faster when the flow rate increases from 0.01 m/s to 0.1 m/s. However, when the flow rate further increases, the phase change rate is almost constant. It can be explained that when the flow rate is small, increasing the flow rate allows more heat to be transferred to the PCM for storage as shown in Fig. 8(d). When the flow rate is larger, the excess heat cannot be absorbed by the PCM due to the limited heat storage rate of the PCM.

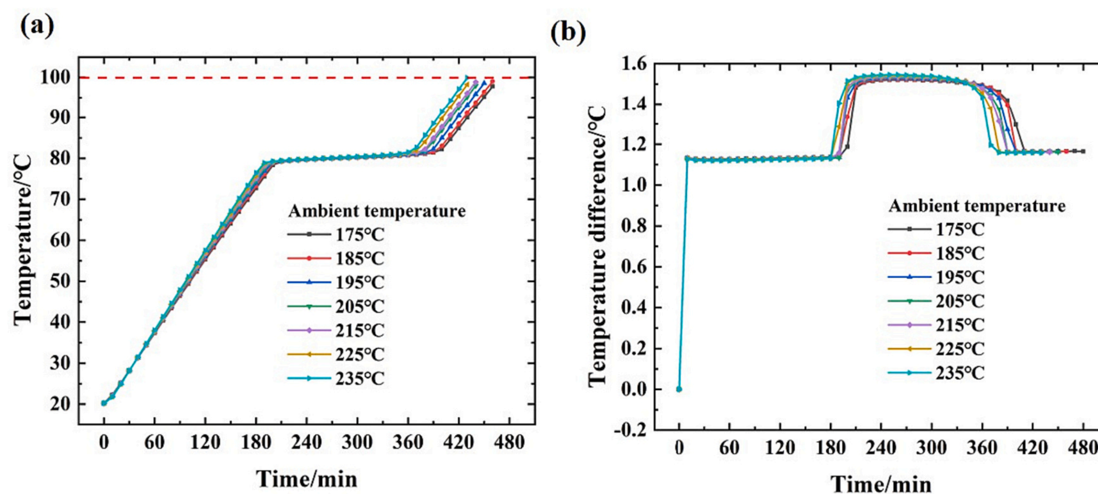

Fig. 11. (a) The temperature-rising of the electronics with time for different ambient temperature; (b) the temperature difference between the electronics and PCM with time for different ambient temperature.

The excess heat is uniformly dissipated throughout the system, resulting in a small temperature difference between the electronics and the PCM. Therefore, the flow rate affects the temperature control of electronics in two main aspects: (1) Increasing flow rate promotes the rapid heat storage of PCM; (2) Increasing flow rate enhances the temperature uniformity of the system.

3.3. Effect of spiral pipe spacing inside the PCM

Due to occupying a certain volume, the spiral pipe spacing inside the PCM affects the heat storage rate and the heat storage amount of PCM. Fig. 9(a) displays the temperature-rising of the electronics with time for different spiral pipe spacing inside the PCM. The temperature of the electronics underwent three stages: rapid rise, almost constant, and rapid rise again. When the spiral pipe spacing is reduced, the temperature-rising rate of the electronics accelerates in the first stage. However, the constant temperature region becomes shorter in the second stage. The electronics can work for the longest time of 450 min when the spiral pipe spacing inside the PCM is 40 mm.

Fig. 9(b) shows the temperature difference between the electronics and PCM with time for different spiral pipe spacing inside the PCM. The temperature difference gradually decreases with the reduction of spiral pipe spacing due to the increase of heat exchange area. The temperature difference reaches 1.47 °C when the pitch was 10 mm. Fig. 9(c) shows the phase change volume fraction with time for different spiral pipe spacing inside the PCM. Compared with others spiral pipe spacing, the longest phase transition interval is 180–390 min with the spiral pipe spacing of 160 mm. Fig. 9(d) displays the heat storage of PCM for different spiral pipe spacing. When the spiral pipe spacing increases from 10 mm to 160 mm, the heat storage capacity of the PCM increases from 505.85 kJ to 568.90 kJ. In summary, it can be concluded that the system possesses best temperature control effect when the spiral pipe spacing is 40 mm.

3.4. Effect of heating power

The heating power affects the heat storage and the heat transfer thermal resistance of the system, which in turn affects the working time of the system. Fig. 10(a) shows the temperature rise of the electronics with time for different heating power. As the heating power decreases, the temperature-rising of the electronics becomes slower, and the constant temperature region becomes significantly longer. When the heating power is reduced from 50 W to 10 W, the temperature-rising rate in the first stage decreases from 27.67 °C/h to 8.46 °C/h, the length of the constant temperature area in the second stage increases from 120 min to 410 min, and the final working time increases from 290 min to 980 min. It can be explained that when the heating power is reduced, the heat storage per unit time of PCM becomes smaller, resulting in a longer workable time. In addition, it can be found that the workable time does not vary linearly with the heating power. When the power becomes larger, the working time becomes shorter. The magnitude of the shortening gradually becomes smaller with the increase of heating power.

Fig. 10(b) shows the temperature difference between the electronics and PCM with time for different heating power. The temperature difference between the electronics and PCM increases by a small amount as the heating power becomes larger. The heating power increases from 10 W to 50 W, and the temperature difference rises only about 2 °C. This means the liquid cooling system can quickly and efficiently transport the heat to the PCM for storage. Overall, the effect of heating power on the workable time is mainly through influencing the amount of heat storage in the system.

3.5. Effect of ambient temperature

Since the temperature downhole is not constant, it is useful to know the effect of the ambient temperature on the system to guide the actual operation. Fig. 11(a) shows the temperature-rising of the electronics with time for different ambient temperature. As the ambient temperature increases from 175 °C to 235 °C, the heat transfer from the high temperature environment to the inside of the vacuum flask is increased. Therefore, the phase transition interval of PCM is advanced and the region becomes shorter, and the final workable time is reduced from 460 min to 440 min. In addition, as the ambient temperature-risings, the temperature-rising of the electronics becomes faster by a relatively smaller amount.

Fig. 11(b) shows the temperature difference between the electronics and PCM with time for different ambient temperature. The temperature difference between the electronics and PCM is almost constant with the increase of ambient temperature. It can be explained that the good thermal insulation of the vacuum flask leads to small influence of the ambient temperature on the internal temperature distribution. In summary, the workable time of the electronics varies less with the ambient temperature due to the excellent thermal insulation of the vacuum flask and insulator.

4. Conclusions

We proposed a hybrid thermal management system for downhole electronics combining liquid cooling and low melting point alloy. The proposed system enhanced the heat transfer through liquid cooling of the spiral and S-shape pipes. Based on several reasonable assumptions, a numerical model for the proposed system was established to simulate the complex heat transfer processes. The accuracy is validated by comparing with the reported experimental results. The performance of the proposed system was furtherly analysed. The conclusion are as follows.

(1) Compared to thermal channels, the heat transfer between the heat sources and PCM is significant enhanced through liquid cooling. The workable time is increased by 220 min. The maximum temperature between the heat sources and PCM reduced more than 28 °C. Compared with previous researches, the liquid cooling cycle combined with PCM can significantly reduce the heat transfer thermal resistance from the heat source to the PCM, and extend the electronics' workable time.
(2) The temperature performance of the system is enhanced with the increase of flow rate. At a flow rate of 0.5 m/s, the maximum temperature difference between the heat source and the phase change material is only 1.59 °C. The temperature control performance of the whole system is strengthened and then weakened with the increase of spiral pipe spacing, with the best one of 40 mm.
(3) The workable time decreases with the increase of heating power, and the electronics only works 290 min with the heating power of 50 W. The workable time of the electronics varies less with the ambient temperature due to the excellent thermal insulation of the vacuum flask and insulator. As the ambient temperature increases from 175 °C to 235 °C, the final workable time is only reduced from 460 min to 440 min.

In the future, the numerical method is expected to be applied for the design and optimization of the hybrid thermal management for actual logging tools. It is noted that the thermal insulation and heat storage design of this work has not yet achieved the best temperature control performance. Suitable optimization method should be proposed for optimizing the structural design in the subsequent work.

CRediT authorship contribution statement

Jiale Peng: Conceptualization, Methodology, Investigation, Writing – original draft. **Chao Deng** & **Fulong Wei**: Data curation, Methodology. **Siqi Ding** & **Run Hu**: Discussion. **Xiaobing Luo**: Conceptualization, Supervision, Writing – review & editing, Funding acquisition.

Declaration of competing interest

The authors declare that they have no known competing financial interests or personal relationships that could have appeared to influence the work reported in this paper.

Data availability

Data will be made available on request.

Acknowledgement

This research is supported by the National Natural Science Foundation of China (51625601) and the Science and Technology Program of Hubei Province (2021BLB176).

References

[1] L.J. Bernard, S. Dyer, A. Harrison, M. Arena, W. Luckett, Testing oilfield technologies for wellsite operations, Oilfield Review 17 (4) (2005) 58–67.
[2] D. Ambrus, V. Bilas, D. Vasic, A digital tachometer for high-temperature telemetry utilizing thermally uprated commercial electronic components, IEEE Trans. Instrum. Meas. 54 (2005) 1361–1365.
[3] W.E. Odiete, New wellbore temperature control design for preventing failure and poor performance of logging tools in high pressure – high temperature wells, Heliyon 8 (2022), e9404.
[4] D. Li, L. Huang, Y. Zheng, Y. Li, P. Wannamaker, J. Moore, Feasibility of source-free DAS logging for next-generation borehole imaging, Sci. Rep. 12 (2022) 11910.
[5] Y. Suzuki, T. Akatsuka, Y. Yamaya, N. Watanabe, K. Okamoto, K. Osato, T. Kajiwara, Y. Ogawa, T. Mogi, N. Tsuchiya, H. Asanuma, Estimation of an ultra-high-temperature geothermal reservoir model in the Kakkonda geothermal field, northeastern Japan, Geothermics 105 (2022), 102525.
[6] J. He, Q. Wang, J. Wu, Y. Zhang, W. Chu, Hybrid thermal management strategy with PCM and insulation materials for pulsed-power source controller in extreme oil-well thermal environment, Appl. Therm. Eng. 214 (2022), 118864.
[7] J. Fang, X. Zhang, L. Li, J. Zhang, X. Shi, G. Hu, Research progress of high-temperature resistant functional gel materials and their application in oil and gas drilling, Gels 9 (2023) 34.
[8] T.J. Lee, High pressure-high temperature well logging and measurements as an emerging technology for geothermal development, Journal of the Geothermal Research Society of Japan 41 (2019) 45–51.
[9] E.H. Amalu, N.N. Ekere, R.S. Bhatti, High temperature electronics: R&D challenges and trends in materials, packaging and interconnection technology, in: 2009 2nd International Conference on Adaptive Science & Technology (ICAST), IEEE, Accra, Ghana, 2009, pp. 148–155.
[10] M.H. Wei, W. Cai, M.Z. Xu, S. Deng, Active cooling system for downhole electronics in high-temperature environments, Journal of Thermal Science and Engineering Applications 14 (2022).
[11] H.J.I. Benedict, Cooling systems for borehole tools, Journal of Geological Resource and Engineering. 1 (2013) 55–60.
[12] H.J.I. Benedict, Development of a cooling system for geothermal borehole probes, Journal of Earth Science and Engineering. 4 (2) (2013) 73–79.
[13] W. Gao, K. Liu, X. Dou, L. Zhang, S. Tang, Numerical investigation on heat transfer rate from the outside environment into the electronic compartment of the measurement-while-drilling tools, Heat Transfer 50 (6) (2021) 5835–5852.
[14] W. Gao, K. Liu, X. Dou, S. Tang, L. Zhang, Numerical investigation on cooling effect in the circuit cabin of active cooling system of measurement-while-drilling instrument based on split-Stirling retirgerator, Case Studies in Thermal Engineering 28 (2012), 101621.
[15] S. Soprani, A.J. Nørgaard, C. Nesgaard, K. Engelbrecht, Design and testing of a heat transfer sensor for well exploration tools, Appl. Therm. Eng. 141 (2018) 887–897.
[16] R. Weerasinghe, T. Hughes, Analysis of thermal performance of geophonic down-hole measuring tools; a numerical and experimental investigation, Appl. Therm. Eng. 137 (2018) 504–512.
[17] A. Sinha, Y. Joshi, Application of thermoelectric-adsorption cooler for harsh environment electronics under varying heat load, Journal of Thermal Science and Engineering Applications 2 (2) (2010) 021004-1–021004-9.
[18] B. Shang, Y. Ma, R. Hu, C. Yuan, J. Hu, X. Luo, Passive thermal management system for downhole electronics in harsh thermal environments, Appl. Therm. Eng. 118 (2017) 593–599.
[19] W. Lan, J. Zhang, J. Peng, Y. Ma, S. Zhou, X. Luo, Distributed thermal management system for downhole electronics at high temperature, Appl. Therm. Eng. 180 (2020), 115853.
[20] J. Peng, W. Lan, Y. Wang, Y. Ma, X. Luo, Thermal management of the high-power electronics in high temperature downhole environment, in: 2020 IEEE 22nd Electronics Packaging Technology Conference (EPTC), Singapore, 2020, pp. 369–375.
[21] J. Kim, J. Lee, T. Song, Vacuum insulation properties of phenolic foam, Int. J. Heat Mass Transf. 55 (2012) 5343–5349.
[22] W. Villasmil, L.J. Fischer, J. Worlitschek, A review and evaluation of thermal insulation materials and methods for thermal energy storage systems, Renew. Sust. Energ. Rev. 103 (2019) 71–84.
[23] X. Li, C. Peng, L. Liu, Experimental study of the thermal performance of a building wall with vacuum insulation panels and extruded polystyrene foams, Appl. Therm. Eng. 180 (2020), 115801.
[24] M.T. Agne, P.W. Voorhees, G.J. Snyder, Phase transformation contributions to heat capacity and impact on thermal diffusivity, thermal conductivity, and thermoelectric performance, Advanced Materials 31 (2019) 1902980.
[25] B. Shang, J. Hu, R. Hu, J. Cheng, X. Luo, Modularized thermal storage unit of metal foam/paraffin composite, Int. J. Heat Mass Transf. 125 (2018) 596–603.
[26] B. Shang, R. Wu, J. Hu, R. Hu, X. Luo, Non-monotonously tuning thermal conductivity of graphite-nanosheets/paraffin composite by ultrasonic exfoliation, Int. J. Therm. Sci. 131 (2018) 20–26.
[27] W. Lan, B. Shang, R. Wu, X. Yu, R. Hu, X. Luo, Thermally-enhanced nanoencapsulated phase change materials for latent functionally thermal fluid, Int. J. Therm. Sci. 159 (2021), 106619.
[28] L. Feng, S. Zhou, Y. Li, Y. Wang, Q. Zhao, C. Luo, G. Wang, K. Yan, Experimental investigation of thermal and strain management for lithium-ion battery pack in heat pipe cooling, Journal of Energy Storage 16 (2018) 84–92.
[29] Y. Fan, X. Zhang, L. Xiang, Y. Cheng, X. Luo, A compact jet array impingement cooling system driven by integrated piezoelectric micropump, Int. J. Heat Mass Transf. 205 (2023), 123905.

[30] X. Wang, B. Li, D. Gerada, K. Huang, I. Stone, S. Worrall, Y. Yan, A critical review on thermal management technologies for motors in electric cars, Appl. Therm. Eng. 201 (2022), 117758.
[31] X. Yang, S. Tan, J. Liu, Thermal management of Li-ion battery with liquid metal, Energy Convers. Manag. 117 (2016) 577–585.
[32] S. Zimmermann, I. Meijer, M.K. Tiwari, S. Paredes, B. Michel, D. Poulikakos, Aquasar: a hot water cooled data center with direct energy reuse, Energy 43 (2012) 237–245.
[33] J.C. Jakaboski, Innovative Thermal Management of Electronics Used in Oil Well Logging, Georgia Institute of Technology, 2004.
[34] S. Ma, S. Zhang, J. Wu, Y. Zhang, W. Chu, Q. Wang, Experimental study on active thermal protection for electronic devices used in deep−downhole−environment exploration, Energies 16 (2023) 1231.
[35] J. Weng, Q. Huang, X. Li, G. Zhang, D. Ouyang, M. Chen, A.C.Y. Yuen, A. Li, E.W. M. Lee, W. Yang, J. Wang, X. Yang, Safety issue on PCM-based battery thermal management: material thermal stability and system hazard mitigation, Energy Storage Materials 53 (2022) 580–612.
[36] J. Peng, Y. Wang, S. Ding, C. Deng, F. Wei, X. Luo, Rapid detection of the vacuum failure of logging tools based on the variation in equivalent thermal conductivity, Int. J. Therm. Sci. 188 (2023), 108245.
[37] J. Peng, W. Lan, F. Wei, C. Deng, B. Xie, X. Luo, A numerical model coupling multiple heat transfer modes to develop a passive thermal management system for logging tool, Appl. Therm. Eng. 223 (2023), 120011.
[38] J.P. Holman, Heat Transfer (10th Edition), McGraw Hill Education, New York, 2009.
[39] L. Song, H. Zhang, C. Yang, Thermal analysis of conjugated cooling configurations using phase change material and liquid cooling techniques for a battery module, Int. J. Heat Mass Transf. 133 (2019) 827–841.
[40] X. Ying, N. Xin, C. Qinglin, D. Zhonghua, L. Xiaoyan, L. Yang, L.I. Cong, Phase-change heat transfer analysis of shutdown overhead pipeline, Case Studies in Thermal Engineering 13 (2019), 100399.
[41] J. Peng, W. Lan, F. Wei, C. Deng, X. Luo, Thermal management for high-power downhole electronics using liquid cooling and PCM under high temperature environment, in: 2022 IEEE 24th Electronics Packaging Technology Conference (EPTC), Singapore, 2022, pp. 935–940.
[42] J. Zhang, W. Lan, C. Deng, F. Wei, X. Luo, Thermal optimization of high-temperature downhole electronic devices, IEEE Trans. Compon. Packag. Manuf. Technol. 11 (11) (2021) 1816–1823.